Chem Soc Rev

This article was published as part of the

2008 Gold: Chemistry, Materials and Catalysis Issue

Please take a look at the full table of contents to access the other papers in this issue

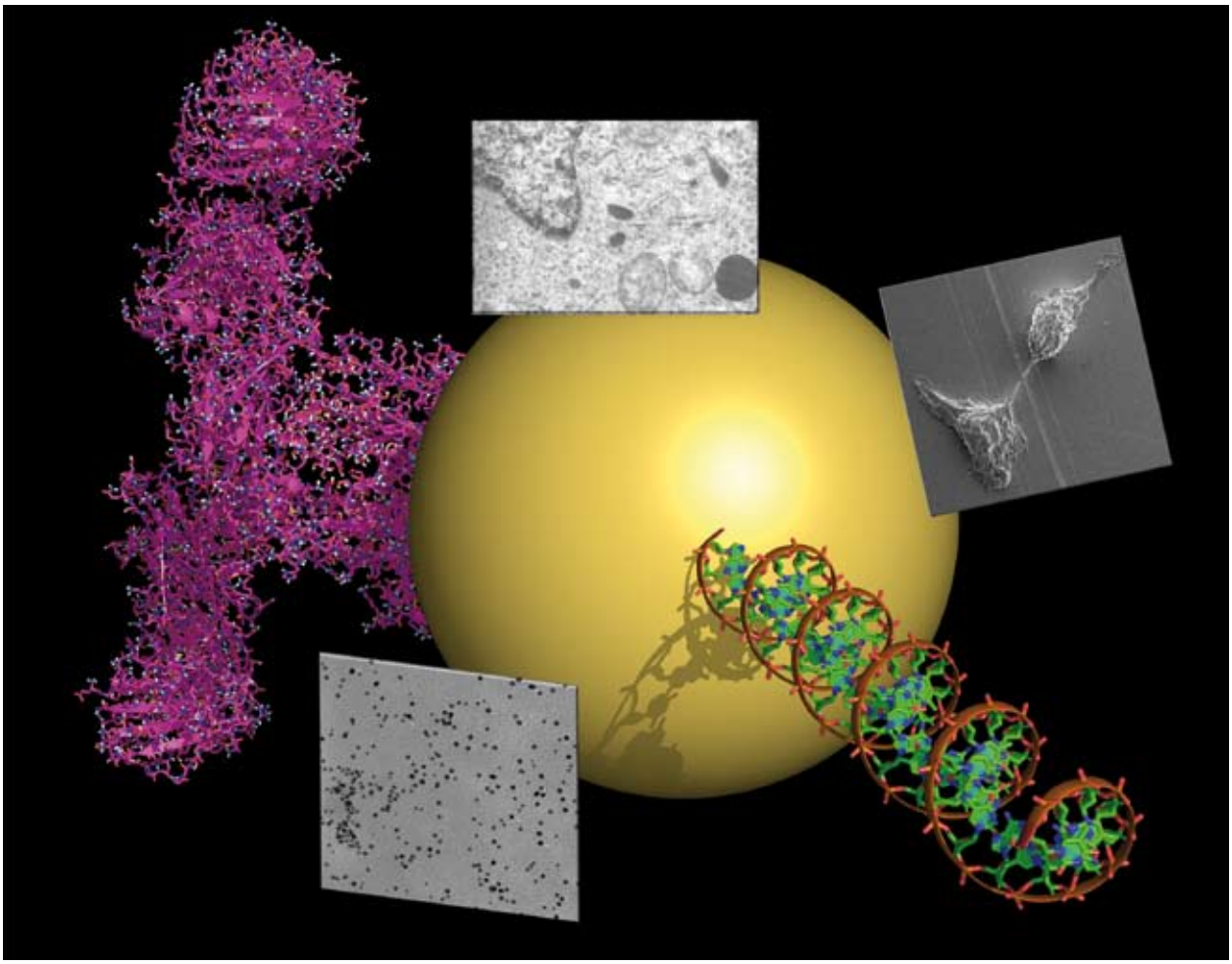

Atomic and electronic structure of gold clusters: understanding flakes, cages and superatoms from simple concepts†

Hannu Häkkinen

Received 19th May 2008
First published as an Advance Article on the web 8th July 2008
DOI: 10.1039/b717686b

Atomic structure and electronic structure are intimately interrelated properties of nanoclusters and nanoparticles, defining their stability, electronic, optical and chemical properties, in other words, their *usability* as potential components for nanoscale devices. This *tutorial review* attempts to describe the development in understanding the structures of bare and ligand-protected gold clusters over the past decade, based on selected density-functional-theory calculations. This review should be of interest both to newcomers in the field and to an interdisciplinary community of researchers working in synthesis, characterization and utilization of ligand-protected gold clusters.

1. Introduction

Gold clusters and nanoparticles exhibit a rich array of interesting and important electronic, optical, chemical and catalytic properties, which has sparked a huge interest in gold-based systems in several interdisciplinary areas, leading to an explosive growth in the volume of both experimental and theoretical research.[1–3] From the theoretical point of view, the chemistry of gold can only be understood if relativistic effects[2] are taken into account properly. This leads to appreciation of the importance of the s–p–d hybridization and the 5d-shell as an active component in making bonds to adsorbing molecules and even to other gold atoms. This fact makes the rich chemistry for gold-based systems. However, bulk gold is a good 6s-free-electron metal, and a natural question arises as to what extent this physical fact shows up in the electronic structure of small clusters or nanoparticles.

Departments of Physics and Chemistry, Nanoscience Center, University of Jyväskylä, FI-40014 Jyväskylä, Finland. E-mail: hannu.hakkinen@phys.jyu.fi; Fax: +358142604758; Tel: +358142604719

† Part of a thematic issue covering the topic of gold: chemistry, materials and catalysis.

Hannu Häkkinen

Dr Hannu Häkkinen received a PhD in 1991 at the University of Jyväskylä (UJ), Finland. He worked for 7 years as a post-doctoral researcher and senior research scientist at the Georgia Institute of Technology, Atlanta. He is currently a professor in computational nanoscience at UJ, a shared Chemistry/Physics position. He has co-authored 35 articles on the theory of gold clusters, nanoparticles and nanowires.

Discussing selected state-of-art calculations, this review shows that buried in the complexity of the details of the 5d–6s derived valence states, there lives a happy population of states that beautifully resembles delocalized electrons in the "jellium" model or the "electrons-in-a-box" model for simple metal clusters.[4] Acknowledging this fact is more than just of academic interest, since the most stable (hence the most "usable") clusters or nanoparticles necessarily have a large energy gap in their electronic structure between the HOMO (highest occupied molecular orbital) and LUMO (lowest unoccupied molecular orbital) levels, and the free-electron behaviour of the highest occupied states is already well developed (as will be shown) for clusters that can have as few as 10 atoms. In those cases, free-electron behaviour determines the overall electronic properties close to the Fermi level, thus being responsible also for low-lying optical excitations or even chemical activity. During the past year, global "conduction-electron" shells have also proven to be the key concept in understanding the thermodynamically stable ligand-protected gold cluster superatoms.

Given the huge body of published work in the area during the past decade, this tutorial review is unavoidably selective, reflecting personal views of the author who has had the privilege of being heavily involved over the past 10 years in an extensive theoretical and experimental collaborative network. At the same time it provides a certain glimpse into the timeline of development of ideas. The discussion starts with the ground-breaking discovery of the unusual tendency of free gold clusters to favour fairly large planar structures, then describes the development of structural motifs from flakes to cages to tubes, and concludes with a discussion of very recent exciting developments in the field of ligand-protected clusters. The author wishes to apologize to researchers who may feel that their work has not received the appropriate attention here, only hoping that another opportunity comes for a more comprehensive treatment of all the relevant literature. In the meantime, readers are referred to many excellent, more comprehensive reviews[3] and complementary papers in this issue of *Chemical Society Reviews*.

2. Gas-phase clusters

2.1 Cationic clusters up to $N = 13$

The first systematic structure determination for a range of cluster sizes came from the Karslruhe group for cationic clusters with $4 \leq N \leq 13$.[5] The structures were determined from combined experimental and theoretical work where the measured collision cross sections in an ion mobility experiment were compared to theoretical (geometrical) cross sections for a large number of relaxed cluster isomers. The structure isomers were found from a combination of consideration of already published geometries for neutral and charged (smaller) simple and noble metal clusters, and from *ab initio* molecular dynamics simulations for the larger sizes (for instance, for Au_{10}^+ more than 30 stationary isomers were produced by the molecular dynamics structure search). The density-functional-theory (DFT) calculations were done by using the BP86 parametrization (Becke–Perdew) for the exchange–correlation potential, a relativistic pseudopotential for $Au(5s^25p^65d^{10}6s^1)$ valence electrons and a localized basis set.

The measured cross sections are shown in Fig. 1 (up to $N = 20$) together with the calculated ones for the energetically most favourable cluster isomers up to $N = 13$. A close-up of the ground-state structures, as well as of close-lying isomers for $N = 6$, 8, 10, is shown in Fig. 2. Comparison to the theory shows that up to $N = 7$ the measured data points essentially coincide with the calculated values for the ground-state structures, all planar: a triangle, a rhombus, an ''hour-glass shape'', a triangle, and a centered hexagon for $N = 3$ to 7, respectively. All of these geometries are simply fragments of a close-packed hexagonal plane. For $8 \leq N \leq 13$, an equally good match is observed for three-dimensional structures, which in many cases can be described as slightly relaxed fragments of fcc

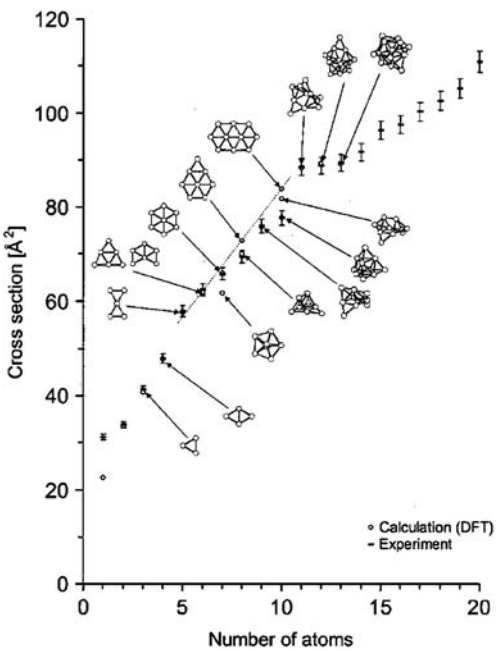

Fig. 1 Measured and predicted ion mobility cross sections for gold cluster cations. Reproduced from ref. 5 by permission. Copyright 2002 American Institute of Physics.

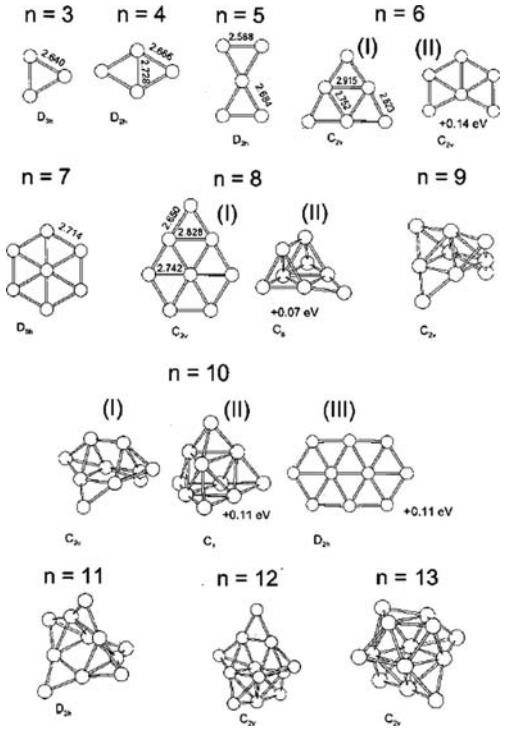

Fig. 2 Calculated low-energy isomers of gold cluster cations. Reproduced from ref. 5 by permission. Copyright 2002 American Institute of Physics.

bulk structure, note *e.g.*, the tetrahedral structure for $n = 10$ (isomer II in Fig. 2). For $N = 8$, 10 a close-lying isomer (8-II and 10-II) gave the best correspondence with the measured cross section. Here, the isomers were within 0.1 eV of the calculated ground state structure. Planar structures 8-I and 10-III, while predicted as being energetically as good as the 3D structures 8-II and 10-II, were not observed in the experiment. This fact set the error bars for theoretical considerations of isomer energetics, assuming that the experimental conditions were such that the thermodynamic ground state structures for each cluster size were obtained and observed. After many more years of studies of (larger) planar anionic clusters, this early-reported discrepancy could now be taken also as an early ''warning sign'' of the tendency of DFT to overestimate the stability of planar gold clusters with gradient-correction approximations (GGA) to the exchange–correlation energy.

2.2 Observation of planar anions up to $N = 12$

In 2001, the Karslruhe group started reporting in scientific meetings observations of fairly large planar cluster anions (with ten or more atoms) from the ion mobility experiment.[6] This experimental result, being clearly at variance with the theoretical predictions known at the time,[7] led to a renewed interest in theoretical studies in the Atlanta group. Structural determinations were soon published in two key reports, the first one (up to $N = 13$) from the Karslruhe group in 2002,[8] being an analogous work to the previous one for cations,[5] and a joint Pacific Northwest Lab (PNL)–Atlanta investigation using photoelectron spectroscopy and DFT for sizes up to $N = 14$.[9] In the meantime, a systematic theoretical study of

noble metal clusters Cu_7^-, Ag_7^- and Au_7^- was carried out in Atlanta,[10] in order to map a more extensive isomer database for heptanuclear clusters than the one used earlier[7] and to understand reasons why the planar structures could be energetically favourable. The stability of the planar structures was traced to strong relativistic effects in bonding in gold,[2] which induce s–d hybridization, contraction of the Au–Au bond length and a significant overlap of d-orbitals.[10,11] Even the choice of the exchange–correlation functional was proven to be critical since LDA (local density approximation) was shown to yield compact 3D structures for Au_8.[11]

The Karslruhe work[8] convincingly set the 2D–3D transition size to $N = 12$. For $N = 12$, a bimodal arrival time distribution was observed and two distinct cross sections measured, allowing for a conclusion that for this cross-over size both planar and three-dimensional structure isomers were present in the beam. It was concluded that for all the other sizes only one isomer was observed. For most cases, the ground state structure predicted by DFT gave also the best fit to the experimental cross section, exceptions included 4-, 10- and 13-atom clusters where the first isomer above the ground-state gave the best fit. Similarly to the reported work on cations,[5] this work indicated that the BP86 functional may overestimate the stability of planar clusters (a planar structure was predicted to be the ground state of Au_{13}^-, but was not observed in the beam). It was also shown that the vertical detachment energy (VDE), which was used extensively before[7] in order to assign theoretical structures to experimentally detected ones, could be used to rule out structure candidates, but it alone cannot give a definite structure assignment as several isomers even with different dimensionality may yield similar VDE values.

In the PNL–Atlanta collaboration,[9] measured high-resolution photoelectron spectra (PES) were compared to theoretically determined density of single-electron states (DOS) for an extensive set of cluster isomers in the size range $4 \leq N \leq 14$. The DFT calculations were made by using the PBE (Perdew–Burke–Ernzerhof) functional, scalar-relativistic norm-conserving pseudopotentials for $Au(5d^{10}6s^1)$ valence electrons, and a plane-wave basis set with 62 Ry kinetic energy cutoff. In the single-particle interpretation, the measured PES contains information about the distribution of binding energies of valence electrons detached from the cluster by a photon of a known energy.[12] The theoretical counterpart in the framework of DFT is the (single-particle) DOS of the Kohn–Sham electrons. Comparing these two ''fingerprints'' may thus provide a more sensitive measure to judge the presence of a given isomer or isomers in the beam, as compared to making structure assignments based on the collision cross section, which is a single number for a given cluster isomer.

The theoretical work reported in ref. 9 confirmed the energetic stability of the earlier reported planar structures, see Fig. 3 and 4. In addition, comparison to the measured PES data (VDE values and spectral details) gave evidence of isomers that were present in the cluster beam for $N = 4$, 8, 12 and 13. As a prominent example, the theory predicts two planar structures for $N = 10$: a triangular and an elongated close-packed flake, see 10A and 10B in Fig. 3 and 5. The two independent DFT calculations[8,9] gave a consistent result by

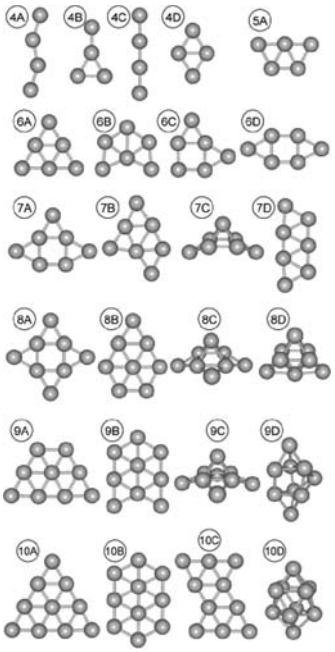

Fig. 3 Calculated low-energy isomers for gold cluster anions, $4 \leq N \leq 10$. The ''A'' structures have the lowest energy. Adapted from ref. 9 by permission. Copyright 2003 American Chemical Society.

predicting the triangular structure 10A to be the ground state and the elongated isomer 10B to be 0.12 eV (ref. 9) or 0.15 eV (ref. 8) higher in energy. The geometrical cross section of the isomer 10B fits better with the measured collision cross section. The two structures deviate significantly from each other regarding the VDE value: for the ground state it is

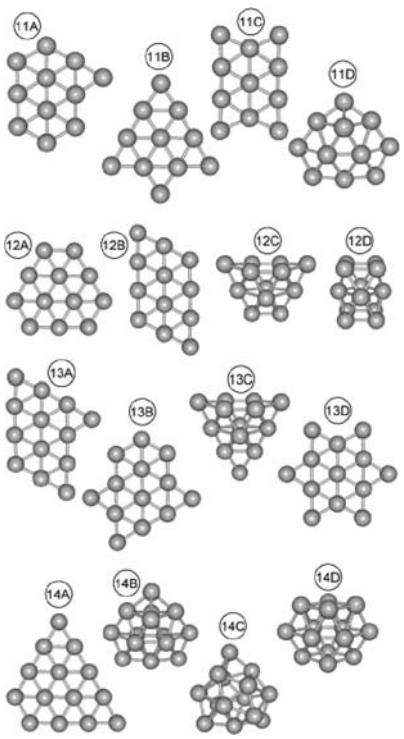

Fig. 4 As Fig. 3 but for $11 \leq N \leq 14$. Adapted from ref. 9 by permission. Copyright 2003 American Chemical Society.

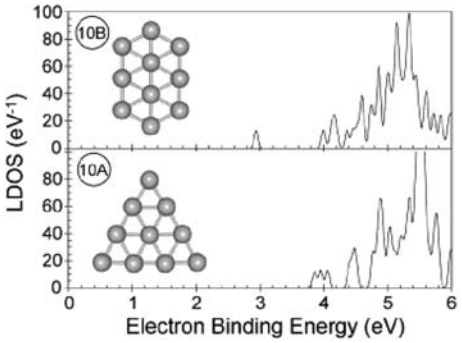

Fig. 5 The theoretical DOS of the two lowest-energy structures of Au_{10}^-. Adapted from ref. 9 by permission. Copyright 2003 American Chemical Society.

calculated to be 3.86 eV (ref. 9) or 4.02 eV (ref. 8) and for the higher-energy isomer it is 2.94 eV (ref. 9) or 3.08 eV (ref. 8). Early PES studies[13] assigned an experimental VDE of Au_{10}^- to be around 3 eV that would be consistent with the higher energy isomeric structure. However, the high-resolution experiment revealed that the low-energy feature in the PES is due to a minor isomer present in the beam and the experimental VDE for the dominant Au_{10}^- structure in the beam was determined to be 3.91 eV which is in excellent agreement with the theoretical VDE values calculated for the ground state.[9] Indeed, by manipulating source conditions and cooling procedures, the first PES feature around 3 eV can be made to disappear[14] which indicates that kinetic effects play a role in the formation processes and possible inter-conversion dynamics of these two planar structures.

The first feature in the measured PES of Au_{12}^- reported from the PNL–Atlanta collaboration has a double-peak structure where the energy difference between the peaks is about 0.1 eV (Fig. 6). This double-peak structure can be interpreted such that the beam has a mixture of the structures 12A, 12B and 12C shown in Fig. 4. The planar structures 12A and 12B have about 0.15 eV higher VDE values than the 3D structure 12C. The corresponding structures 12-I (= 12A) and 12-II (= 12C) were reported also in ref. 8 to be responsible for the two observed collision cross sections. The isomer 12B was not reported in ref. 8, and its theoretical cross section was not calculated. It is extremely interesting to note that also for $N = 12$, it is possible to manipulate the beam conditions such that the relative intensities of the two peaks in the double-peak feature can be changed.[14] Again, this indicates the importance of kinetic effects in the formation of the isomers of this 2D–3D cross-over cluster size. If the predicted (GGA-DFT) large energy gap (0.5–0.7 eV) between the structures 12A and 12C is taken seriously, the co-existence and relative abundances of 2D and 3D $N = 12$ clusters in the beam is probably due to completely different formation routes (nucleation from already planar or three-dimensional seeds of $N \neq 12$) rather than from the inter-conversion dynamics. A DFT-based tight-binding molecular dynamics study added a new dimension to interpretations of cluster kinetics upon cooling: simulations of the cooling process showed that in the 2D–3D crossover region, supercooling to "wrong dimensionality" is possible.[15] A very recent DFT study addressed once more the issue of the accuracy of exchange–correlation functionals and claimed that improvements over the conventional GGA level (*e.g.* PBE) are needed to gain a more realistic description of the energetics among planar and 3D gold cluster isomers.[16] The situation still remains somewhat unsatisfactory due to the fact that benchmark calculations using correlated many-body methods are not possible at the moment for clusters beyond 10 atoms, and "calibrating" DFT results against experimental data is always dangerous.

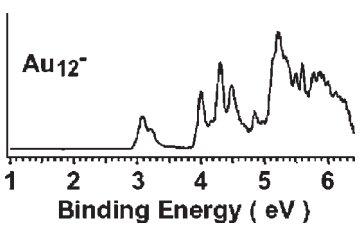

Fig. 6 The experimental PES of Au_{12}^-. The double-peak feature of the first peak signals the presence of isomers in the beam. Adapted from ref. 9 by permission. Copyright 2003 American Chemical Society.

The question remains why the odd-valence-electron cluster Au_{10}^- breaks the usual odd–even alternation in the VDE pattern by having a high VDE value for its D_{3h} ground-state configuration (Fig. 7). The answer can be found by inspecting the relevant highest occupied Kohn–Sham orbitals (Fig. 8). Analysis of the major angular momentum character[17] of these orbitals shows that they are of the 2S and 1D type, very analogous to orbitals that electrons would have in a planar harmonic quantum dot with a triangular shape.[18] In that model, a major electron shell closing is at 12 electrons in a configuration $1S^21P^42S^21D^4$. For Au_{10}^-, 1S and 1P symmetries can also be found from states that are deeper in the energy spectrum, partially mixed with the Au(5d) derived band. Consequently, Au_{10}^- with its 11 Au(6s)-like "conduction electrons" is just one electron shy of gaining the shell closure, which explains the high VDE of its D_{3h} ground state. It is also observed that the neutral Au_{10} is a spin-triplet, manifesting Hund's rule in operation for the degenerate 1D states. Thus, neutral D_{3h} Au_{10} exhibits "accidental magnetism" due to the symmetry.

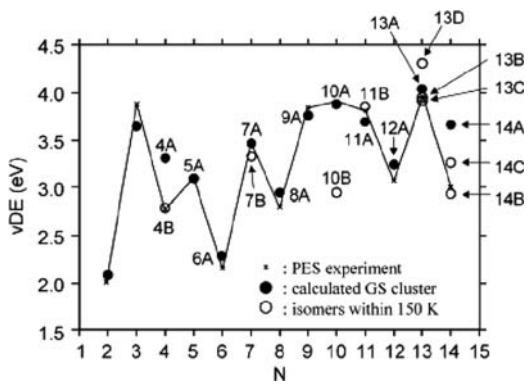

Fig. 7 Comparison of experimentally determined VDE values (solid line) to calculated ones (symbols, isomer labeling from Fig. 3 and 4). Reproduced from ref. 9 by permission. Copyright 2003 American Chemical Society.

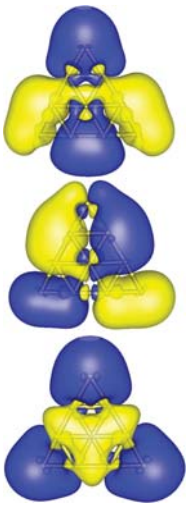

Fig. 8 Visualization of some of the highest Kohn–Sham orbitals for the D_{3h} Au_{10}^- ground-state cluster (10A in Fig. 3 and 5). 2S and 1D symmetries are seen.

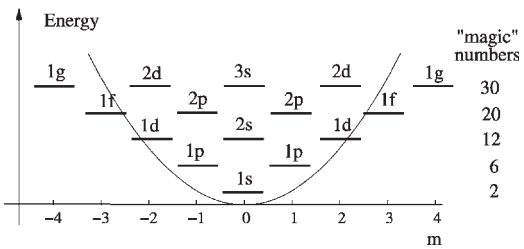

Fig. 9 A schematic of the electron states in a planar harmonic quantum dot.

Further evidence of the applicability of the planar quantum-dot model for planar gold clusters follows. Fig. 9 shows a schematic energy level diagram for the quantum-dot model. After shell closure at 12 electrons, a new 8-electron shell opens with 2P and 1F symmetries, leading to the next "magic number" in a plane, 20. Fig. 10 shows the two highest occupied orbitals for D_{3h} Au_{12}^- (the ground-state geometry). The effective 6s-electron count is now 13. Indeed the highest state, the singly-occupied SOMO shows a beautiful 1F symmetry and the state below that has a clear 2S symmetry of the 6-electron 2S1D shell. This shell closing is responsible for the large HOMO–LUMO gap in neutral Au_{12}, visible in the experimental photoelectron spectrum of the anion.[9]

The planar quantum-dot model works well even for gold clusters supported by a large-band-gap oxide, such as MgO.[19] Fig. 11 shows a neutral Au_{13} cluster adsorbed at a color center

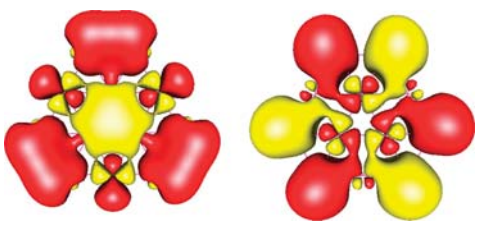

Fig. 10 Left: HOMO−1 state of the D_{3h} Au_{12}^- cluster (structure 12A in Fig. 4). Right: the HOMO state. 2S and 1F symmetries are seen.

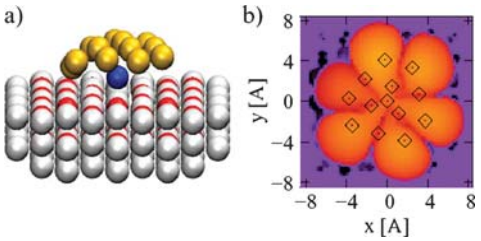

Fig. 11 (a) Au_{13} cluster adsorbed on a color center of the MgO surface (the blue Au atom pins the cluster to the defect). (b) Simulated STM image formed from the density of the SOMO of the gold cluster. Adapted from ref. 19 by permission. Copyright 2007 American Physical Society.

(oxygen vacancy) of MgO and a theoretical STM image at low negative bias voltage, constructed from the density of a single electron state, the SOMO state of the system, which lies in the band gap of MgO. The image visualizes the 1F symmetry of the SOMO. In the same work, theoretical STM images for Au_{20} adsorbed on the color center of MgO were also calculated, showing the symmetries of HOMO (2P) and LUMO (1G) states of the gold cluster.

2.3 From flakes to cages to tubes: clusters with N = 13–24

Two recent experimental investigations for larger anionic clusters, a photoelectron study[17] and an electron diffraction study,[20] confirmed the early conclusions from mobility experiments regarding the 2D–3D structural cross-over at the size Au_{12}^-. The experimental data were compared to the corresponding theoretical quantities using the same isomer database.[17] These studies confirmed the earlier photoelectron results for tetrahedral structures of Au_{16}^- [21] and Au_{20}^-.[22] Furthermore, these investigations showed the gradual transformation of the optimal structure from a near-planar, flat "cage" (N = 13, 14) to a tetrahedral cage, evolving finally to tubular structures for $N \geq 20$.

Fig. 12 shows the energy-level diagram of Kohn–Sham states for anions with N = 16, 18, 20, and visualization of selected orbitals for Au_{20}^- (the special Au_{16}^- case is discussed

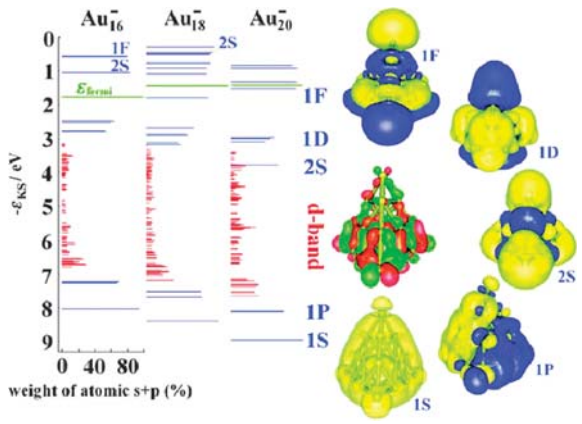

Fig. 12 Left: angular-momentum analysis of Kohn–Sham eigenstates for Au_{16}^-, Au_{18}^- and Au_{20}^-. The states marked by blue have high local sp weight on atoms, globally they are free-electron-states over the cluster. A visualization of such states for Au_{20}^- is on the right. Reproduced from ref. 17 by permission. Copyright 2007 Wiley.

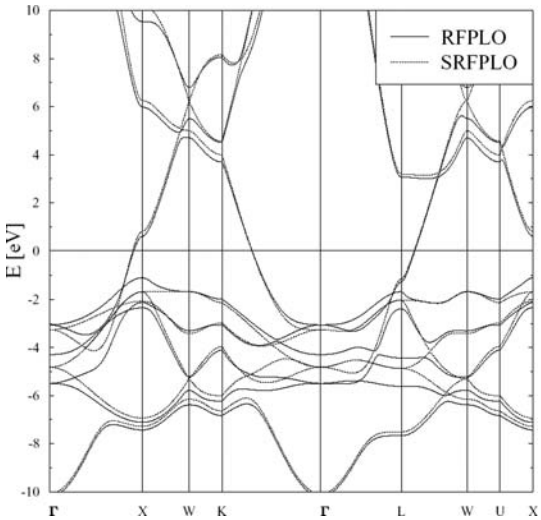

Fig. 13 Calculated band structure of bulk gold, from relativistic (R) or scalar-relativistic (SR) full-potential calculation (FPLO). Adapted from ref. 23.

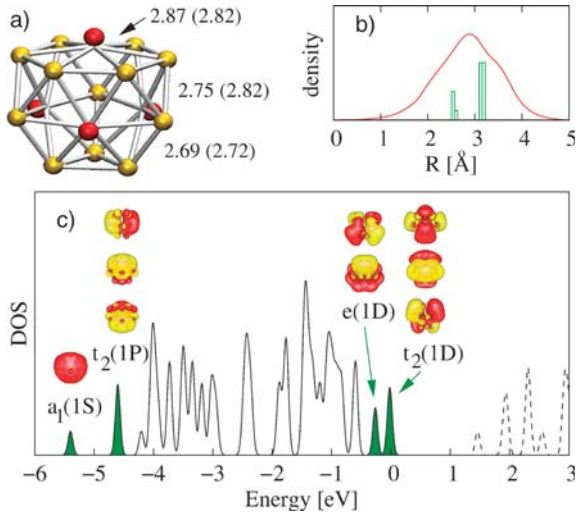

Fig. 14 (a) Structure of Au_{16}^{q}. The numbers are values of the indicated Au–Au distances in the dianion, $q = -2$ (in parentheses for the cation, $q = +1$). The "stick" framework indicates the structure of the cation, and the "balls" are drawn from the coordinates of the dianion. Only the red face atoms move significantly during relaxation between different charge states. (b) Radial distribution of atoms (bars) and electrons (line) for the dianion. The radius of the cage is ~2.5 Å. (c) Density of Kohn–Sham molecular orbitals (DOS, folded by 0.05 eV Gaussians) of Au_{16}^{2-}. The HOMO state is at zero energy, and the empty states are denoted by a dashed line. The shaded and labeled peaks denote the delocalized, T_d crystal field split states that are derived from a hollow jellium confinement (jellium labeling in parentheses). These MO's are also visualized. t_2 is the 6-fold degenerate HOMO orbital (3 spatial orbitals × 2 for spin). Reproduced from ref. 24 by permission of the PCCP Owner Societies 2006.

in the next section). Angular momentum analysis of the orbitals of Au_{20}^{-} shows that they can be generally divided into two major classes, the Au(5d) derived "band" of states in the energy range −3 eV to −8 eV, and to delocalized Au(6s) derived "jellium-like" states above and below the 5d-band. Qualitatively, this medium-size cluster already shows all the characteristics of the bulk band of gold, where the free-electron-like 6s-derived band crosses the 5d-derived band and extends all the way from the gamma-point to the Fermi surface (Fig. 13).[23] The upper edge of the 5d-band is about 2 eV below the Fermi surface, which also qualitatively matches the behaviour of the states in the Au_{20}^{-} cluster. The Au_{20}^{-} then shows the expected free-electron-like shell filling pattern of 21 electrons: $1S^2 1P^6 2S^2 1D^{10} 1F^1$, with $1F^1$ as a SOMO, confirming that the large HOMO–LUMO gap of the neutral Au_{20} is the "jellium gap" between 20 and 21 electrons. Many more examples of the free-electron-behaviour of medium-size gold clusters can be analyzed, and some are given below.

2.4 Au_{16}^{-}: the smallest golden cage and the manifestation of 18 delocalized electrons

In 2006, a combined photoelectron spectroscopy and density functional study[21] concluded that the experimentally observed isomer of the Au_{16}^{-} anion has tetrahedral symmetry and the geometry can be derived from the previously discovered[22] T_d-symmetric Au_{20}^{-} by removing the four vertex atoms and allowing for an outward relaxation of the 4 face-centered atoms, which yields a structure that was coined as the "smallest golden cage" (see Fig. 14).

Since the early 1990's it had been known that Au_{16}^{-} exhibits high VDE,[13] breaking the odd–even alternation just as Au_{10}^{-} discussed above. In a follow-up study, it was shown that the high VDE of Au_{16}^{-} is due to a tendency to complete a shell of 18 delocalized electrons leading to stability of the dianionic Au_{16}^{2-} cluster with a predicted HOMO–LUMO gap of 1.5 eV.[24] In jellium-like notation, the relevant shells are $1S^2 1P^6 1D^{10}$ with the 1D shell split by the symmetry. In terms of the T_d-symmetric crystal-field split molecular orbitals, the relevant configuration is $a_1^2 t_2^6 e^4 t_2^6$. The 2S shell is at high energies (and thus unoccupied) due to the fact that a radial node is not supported by the hollow cage. The cage maintains its robust geometry, with a minor Jahn–Teller deformation, over several charge states ($q = -1, 0, +1$), forming spin doublet, triplet and quadruplet states according to Hund's rules. The cage is roomy enough so that it can be doped endohedrally by atoms like Si or Al.

It is naturally possible to continue filling angular-momentum shells in a hollow cage geometry by neglecting all orbitals that would include a radial node. In that case, the expected shell closings are at 32 ($18 + 1F^{14}$), 50 ($32 + 1G^{18}$) and 72 ($50 + 1H^{22}$) electrons and all are shown to lead possible metastable isomers of icosahedral symmetry for Au_{32}, Au_{50} and Au_{72}.[25–27] The author of this review however does not expect these metastable structures to be relevant in gold chemistry. On the other hand, it may be of interest to study T_d hollow cages for Cu_{16}^{-} and Ag_{16}^{-}, as the early experiments showed that they too have high VDE like Au_{16}^{-}.[13] The explanation should be found in the closure of the 18 electron shell in a hollow cage.

2.5 Medium-size gas-phase clusters

Since the early 1990's, the Au_{34}^{-} anion has been known to have a very large gap in the photoelectron spectrum,[13] reflecting a large HOMO–LUMO gap for the corresponding neutral

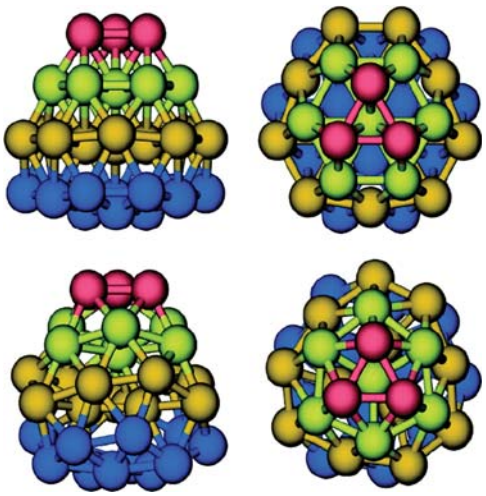

Fig. 15 Two views of predicted low-energy C_{3v} (top) and C_3 (bottom) structures of Au_{34}^-. The C_3 structure gives the best match with experimental electron diffraction and photoelectron data. Reproduced from ref. 28 by permission. Copyright 2007 Wiley.

cluster at 34 s-electrons in a configuration $1S^21P^61D^{10}2S^21F^{14}$. A recent combination of electron diffraction, photoelectron spectroscopy and density functional theory calculations shed light onto its most likely atomic structure.[28] The best fit to the measured ED data was found for a C_3 structure that can be constructed from a more symmetric C_{3v} geometry *via* a twist (see Fig. 15), which increases the surface packing density, similar to what has been found for helical gold nanowires.[29]

Four years ago, high-resolution UV-photoelectron spectra of cold mass selected Cu_N^-, Ag_N^- and Au_N^- with N = 53–58 revealed interesting systematic behaviour.[30] It was observed that while the spectra of copper and silver clusters were practically identical in the upper valence band region (corresponding to delocalized electron shells 2P and 1G), gold clusters exhibited a totally different spectral structure with only one, although much-detailed, band (Fig. 16). The series of highly degenerate peaks for Cu and Ag is a signature of high symmetry in the atomic structure. Indeed, by comparing the experimental PES to theoretical DOS calculated for several candidate structures, it was unambiguously concluded that copper and silver clusters in that size range have 55-icosahedron based ground-state structures (Fig. 17). On the other hand, several low-lying, low-symmetry isomers were found for Au_{55}^-. None of these structures produced DOS that would match satisfactorily the observed PE spectral features. It is possible that the true ground-state structure was not found or that in reality there are many low-energy structures present even at low temperatures (around 200 K). The preference for Au_{55}^- to have low-symmetry structures as opposed to symmetric ones was traced to relativistic bonding effects. Finally, one can remark that the highly *symmetric* Au_{55}^- metastable isomers, like an icosahedron, support beautiful degenerate peaks of 2P and 1G jellium states (1G split by the I_h symmetry as for Ag_{55}^- and Cu_{55}^-). The large energy gap at around 5 eV electron binding energy in Fig. 17 for I_h Au_{55}^- can be identified as the "34 electron gap". This fact has relevance for the discussion of symmetric cores of ligand-protected gold clusters below.

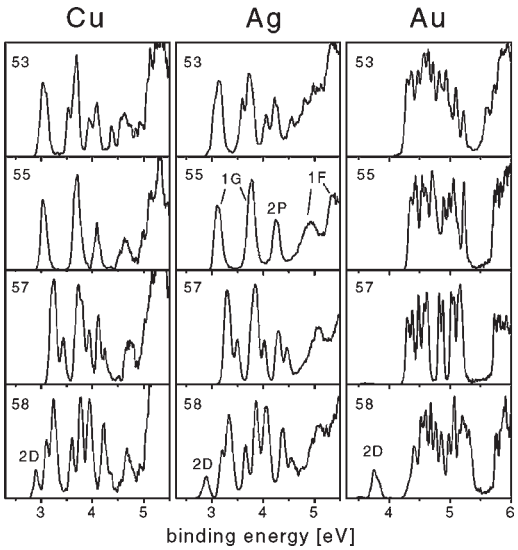

Fig. 16 High-resolution photoelectron spectra from noble metal cluster anions with 53 to 58 atoms. Reproduced from ref. 30 by permission. Copyright 2004 American Physical Society.

3. Ligand-protected nanoparticles

3.1 Early models

Synthesis, characterization and functionalization of size-controlled, ligand-stabilized gold nanoparticles (AuNPs) are long-standing issues in the chemistry of nanomaterials. Ligand-protected AuNPs offer an intriguing possibility to

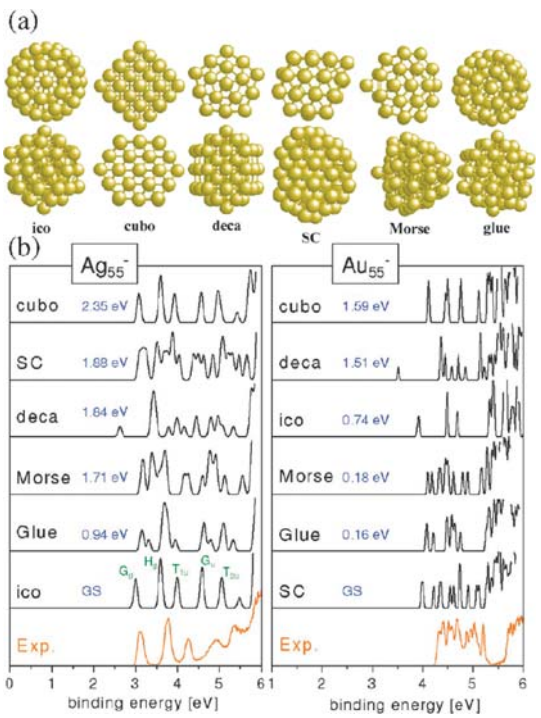

Fig. 17 Theoretical DOS for a number of structure isomers for Ag_{55}^- and Au_{55}^-. Comparison to the experimental PES shows that the observed Ag_{55}^- isomer is the icosahedral one. For gold, none of the structure candidates gives a perfect match. Reproduced from ref. 30 by permission. Copyright 2004 American Physical Society.

economically fabricate building blocks for potential applications in catalysis, sensing, photonics, biolabeling and molecular electronics. These building blocks are known to have distinct size-dependent physical and chemical properties. Collective efforts by several experimental groups have established a series of Au core sizes in the 1 to 3 nm range that are predominantly formed in the process of reducing gold from a metal salt in the presence of phosphines (PR_3) or thiols (HS–R). The ''phosphine chemistry'' was established in the early 1980's[31,32] and the ''thiolate chemistry'' in the mid-1990's.[33]

Concentrating here on thiolate-protected clusters, the early theoretical models around the mid-1990's employed pre-parametrised potential functions for interatomic interactions and structures were explored *via* classical molecular dynamics methods, a considerable computational challenge at the time. A prevailing structural concept was the one with an atomically ''smooth'' Au/S interface and compact gold core. Parameters to describe the Au–S interaction were taken from bulk Au/SAM systems. (We note that the developments in understanding the Au/S interface in SAMs on the basis of the same interface in thiolate-protected clusters commands a separate review and is not discussed here.) Central issues were optimal packing inside the ligand shell, AuNP–AuNP interactions, and AuNP lattices. Much of the work of that era is highlighted in ref. 34 and 35.

The first electronic structure calculations of the protected clusters concentrated on the $Au_{38}(SR)_{24}$ cluster,[36–38] where the structure motif for the Au_{38} core was drawn from classical simulations for medium-sized gold clusters.[35] The optimal binding configuration of thiolates was found for S at Au–Au bridging positions on the symmetric, truncated-octahedral gold core. Dithiolates were not observed to be stable. The Au–S bonding at the Au/S interface was found to involve a significant transfer of electrons from gold to sulfur. Ref. 38 gave the first ''warning signs'' on the possibility that the Au–S interaction may be significantly affected by the choice of the exchange–correlation functional. Soon thereafter, the symmetric structural model was challenged by an investigation that showed significant disturbance of the surface-geometry of Au_{38} by the thiolates, leading to an ''amorphous'' core and a complicated Au–S bonding structure at the interface.[39] This study was largely driven by concurrent DFT investigations of disordered structures of bare medium-sized gold clusters.[40]

3.2 The "Divide and Protect" concept

In 2006, a novel ''Divide and Protect'' structural concept was introduced.[41] The new structural model emerged from density functional calculations with improved exchange–correlation functionals. Calculations with the PBE functional, starting from the symmetrical, compact structures reported earlier[36] spontaneously led to ''etching'' of Au atoms from the Au_{38} core by sulfur, leading to formation of six square-like $(AuSR)_4$ units (Fig. 18). Consequently, the composition $Au_{38}(SR)_{24}$ could be written as $Au_{14}[(AuSR)_4]_6$. The gold atoms in the cluster were found to be in two distinct chemical states, the ones in the Au_{14} core were essentially neutral (''metallic'') and those inside the ''rings'' oxidized (Au^+). The binding energy of

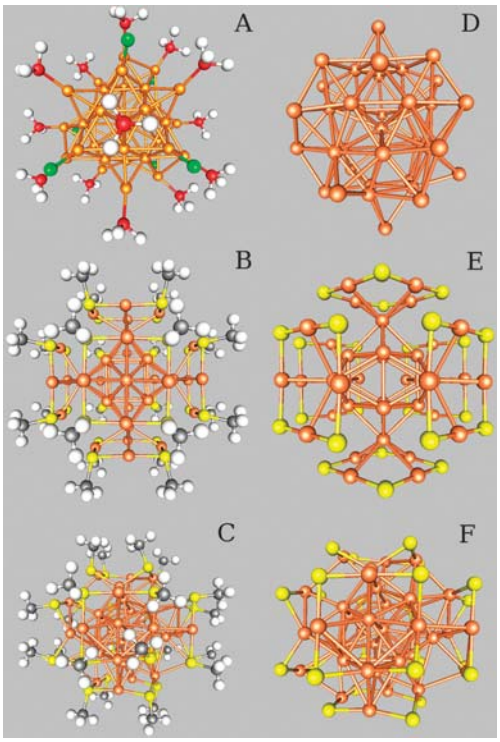

Fig. 18 A: a phosphine–chloride passivated $Au_{39}(PH_3)_{14}Cl_6^-$ cluster; B, C: two isomers of $Au_{38}(SR)_{24}$. D: Au_{39} core, shown by a 90 degree rotation about the horizontal axis on the left; E: Au–S framework of B, with 45 degree rotation about the vertical axis on the left; and F: Au–S framework of C. Au: orange-brown, S: yellow, P: red, Cl: green, C: dark grey, H: white. Reproduced from ref. 41 by permission. Copyright 2006 American Chemical Society.

one $(AuSR)_4$ unit to the Au_{14} core was found to be quite weak, about 1 eV. A follow-up systematic study on the $(AuSR)_x$ units showed that they are polymeric after $x \geq 4$, *i.e.*, the binding energy per one AuSR unit saturates.[42]

Comparison to the earlier alternative structure model with a disordered gold core[39] showed that the new PBE-calculations also modified that structure and a tendency to form distinct $(AuSR)_4$ units was observable (Fig. 18), signaling an energetic competition between two driving factors: to optimize the number of metallic Au–Au interactions and to optimize the number of covalent Au–S interactions. The energetic competition is due to the improved description of the Au–Au interaction strength (it has been known that the early LDA calculations overestimated that interaction significantly). At the improved level, the Au–Au dimer binding energy (both experimental and PBE-predicted) is 2.3 eV whereas the Au–SR bond energy is about 2.5 eV (PBE-value). On the other hand, to create a Au vacancy at the close-packed Au(111) surface in the simplest pair-bond approximation, with 9 bonds broken and 3 new created, one needs $((9-3)/12)\ E_{coh} = 0.5\ E_{coh}$ (E_{coh} is the bulk cohesive energy). The experimental E_{coh} is about 3.8 eV, so only 1.9 eV is needed. It is worth noting here that in ref. 43 it was shown that it is possible to pull monatomic Au chains out of a gold surface *via* a methylthiolate ''clamp''. This provides a direct proof of the strength of the Au–S bond as compared to the Au–Au bond.

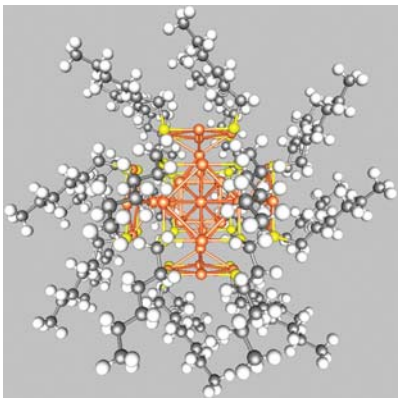

Fig. 19 The "divide and protect" structure motif provides an attractive way to organize long or bulky ligands and minimize steric repulsion. Reproduced from ref. 41 by permission. Copyright 2006 American Chemical Society.

Structurally, the new concept also provided an attractive model for optimized packing in the ligand shell, since steric repulsion among long (such as C12) or bulky (such as glutathione) ligands could be avoided (Fig. 19).

In 2007, a related model ("core-in-cage") was introduced for the $Au_{25}(SR)_{18}$ cluster consisting of a Au_7 core protected by two $(AuSR)_3$ and one $(AuSR)_{12}$ unit.[44]

3.3 The experimental breakthrough and the success of the superatom model for all-thiolate protected clusters

In October 2007, the first-ever total-structure-determination of an all-thiol protected gold nanoparticle was published by the group of R. Kornberg[45] (see also the associated commentary, ref. 46), based on X-ray diffraction at 1.1 Å resolution from single crystals containing a distinct compound with 21 kDa Au core mass, protected by *p*-MBA ligands (*p*-MBA = *p*-mercaptobenzoic acid). Specifically, the composition was determined as $Au_{102}(p\text{-MBA})_{44}$ and the crystal unit cell was observed to contain an enantiomeric pair of these clusters. The structure of $Au_{102}(p\text{-MBA})_{44}$ was shown to exhibit a high degree of five-fold symmetry: a central 49-atom Marks decahedron, capped by two 20-atom caps of C_5 symmetry, extending the number of Au atoms with 5-fold rotational symmetry up to 89. Only the 13 Au atoms forming an "equatorial band" were found to be in irregular positions, and their bonding combination with the *p*-MBA ligands is responsible for the overall chirality of the particle.

A subsequent thorough analysis of the atomic structure and full density functional treatment of the electronic structure of the $Au_{102}(p\text{-MBA})_{44}$ cluster (with all of its 762 atoms and 3366 valence electrons) resulted in a clear picture of the identity of the protecting gold–thiolate ligands and the gold core, and the underlying reasons for the thermodynamic stability of this compound.[47] It was found that the atomic structure of the $Au_{102}(p\text{-MBA})_{44}$ compound (Fig. 20) consists of an approximately D_{5h}-symmetric Au_{79} metallic core with a protective gold–thiolate layer of composition $Au_{23}(p\text{-MBA})_{44}$. Hence $Au_{102}(p\text{-MBA})_{44}$ is more accurately described in the formulation $Au_{79}[Au_{23}(p\text{-MBA})_{44}]$. The gold atoms in the cluster are in two distinct chemical states: the 79 core Au atoms (Au_{core}) are in a metallic (charge-neutral) state whereas the 23 Au atoms (Au_{ligand}) that belong to protecting $RS(AuSR)_x$ units are oxidized. Consequently, the composition evokes the predicted "divide and protect" structure motif.[41] The $Au_{23}(p\text{-MBA})_{44}$ layer can further be decomposed into 19 units with $x = 1$ and 2 units with $x = 2$, which are anchored to the core *via* sulfur in atop positions. The Au_{core}–S–Au_{ligand} angle is close to 90 degrees and the Au_{ligand} atoms are linearly coordinated by two sulfurs. We note here that the concept of a "staple" was introduced in ref. 45 to describe the protecting gold–thiolate unit. A visualization of such "staples" found in $Au_{102}(p\text{-MBA})_{44}$ is shown in Fig. 20. However, in the spirit of the "divide and protect" scheme, the actual protecting units are rather the $RS(AuSR)_x$ where Au is oxidized. The "staples" already include Au^0 atoms from the Au_{79} core. The total number of $RS(AuSR)_x$ units, 21, is intimately related to the electronic stability of the particle.

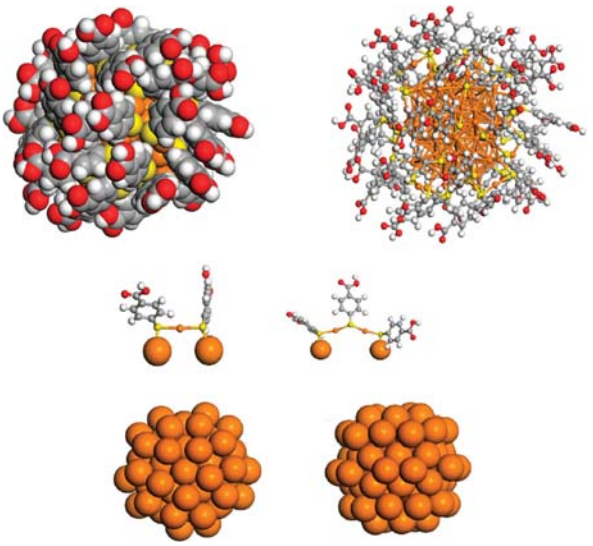

Fig. 20 Top: two views of the $Au_{102}(p\text{-MBA})_{44}$ cluster. Middle: the protecting RSAuSR and $SR(AuSR)_2$ units, bound to core Au atoms (large balls). Bottom: two views of the Au_{79} decahedral core. Au: brown, S: yellow, C: gray, O: red, H: white. After ref. 47.

A confirmation of the metallic character of the Au_{79} core came through analysis of radial difference in the cumulative induced charge when the $Au_{102}(p\text{-MBA})_{44}$ compound was made either cationic or anionic (that is, remove or add one electron, re-calculate the electron density, and analyse the radial density difference). In both cases, the major portion (90%) of the induced charge was found in the $Au_{23}(p\text{-MBA})_{44}$ shell. Virtually no change was observed inside a radius of 5 Å and only 10% of the induced charge resides at the interface between the Au_{79} core and the $Au_{23}(p\text{-MBA})_{44}$ protective layer (5 Å $< R <$ 7 Å). Since a metallic cluster accepts charge only at its surface, it could be directly concluded that the electronic structure of the Au_{79} should feature delocalized-electron shell structure, just as the smaller bare metallic Au clusters discussed earlier.

The calculated HOMO–LUMO gap of the $Au_{102}(p\text{-MBA})_{44}$ cluster was found to be appreciable, about 0.5 eV, indicating a major electron shell closing. The analysis of angular momentum character of the electron states of the bare Au_{79} core and

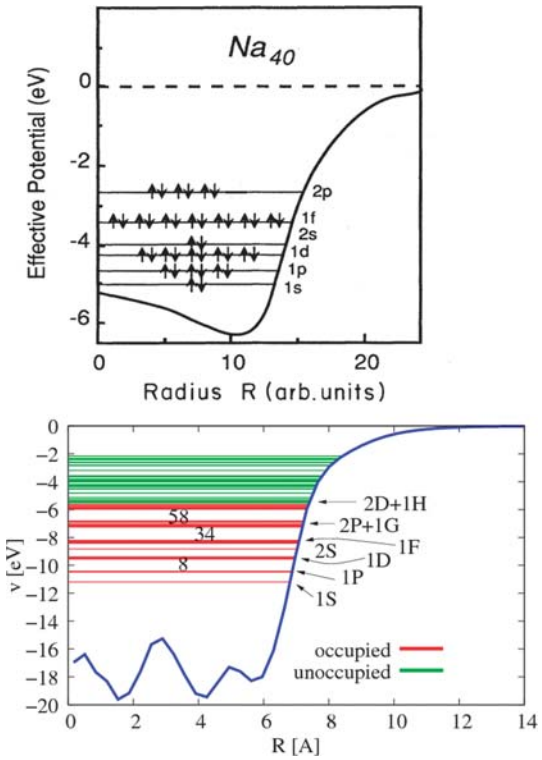

Fig. 21 Top: self-consistent effective potential of jellium sphere corresponding to Na_{40} with the occupation of electron energy levels. Bottom: radially averaged Kohn–Sham potential of the Au_{79} core in $Au_{102}(p\text{-MBA})_{44}$ (6s-only calculation) with the occupied (red) and unoccupied (green) energy levels and their symmetries. Top figure adapted from ref. 4 by permission. Copyright 1993 American Physical Society.

the full compound revealed the exact mechanism of how this shell closing is obtained in the protected cluster.

The bare Au_{79} has an odd number of valence electrons. Its SOMO state lies in the middle of a band that consists of 34 single-electron states, out of which 2 states show the S-symmetry, 10 states D-symmetry and 22 states H-symmetry. This set of states is separated from other states by rather large energy gaps: 0.5 eV gap to deeper-lying (occupied) states with a dominant G-character, and 0.33 eV gap to higher-lying (empty) states with I-character. The symmetries and the energy ordering of the states correspond well to the delocalized conduction-electron model where angular symmetries of 3S, 2D, and 1H appear between major electron shell closings at 58 delocalized electrons and at 92 delocalized electrons. In fact, if one does a model calculation for the bare Au_{79} core just considering Au to be 6s-monovalent metal, the situation may be well compared to the classic case of gas-phase sodium clusters (ref. 4): the core supports all the major gaps expected for a (spherical) 79-electron jellium system: those at 2, 8, 18, 20, 34 and 58 electrons (Fig. 21).

What happens now when the 21 $RS(AuSR)_x$ units interact with the Au_{79}? *Formal* charge counting of such units indicates that they would like to attract one electron each out of the gold core, making the core to be *formally* $Au_{79}^{(21+)}$, justifying the first conjectures of the $(79 - 21 = 58)$-electron shell closure in $Au_{102}(p\text{-MBA})_{44}$ in ref. 45 and 46. In *reality*, the surface-covalent bonds that form between the surface Au^0 atoms of the core and the S atoms of the units were found to be close to charge-neutral. The *net result* with respect to the modifications to the conduction-electron shell structure of the initially bare Au_{79} core is still the same as in the formal charge-counting model: 21 conduction electrons are "used" to make covalent bonds with sulfurs, therefore they "disappear" from the occupied electronic shells and re-hybridize with sulfur states. Therefore one can well characterize the protected $Au_{102}(p\text{-MBA})_{44}$ electronically as a 58-conduction-electron system. It is also interesting to note that this picture of modification of electron shells is very rigid: the 0.5 eV gap at 58 electrons (the HOMO–LUMO gap of the full particle) is the same as found already in the bare Au_{79} core.

All this analysis could be summarized as follows: the stability of the $Au_{102}(p\text{-MBA})_{44}$ particle is due to several co-existing factors: (i) formation of a compact, symmetric-enough metal core that can support clear electron-shell structure, (ii) complete chemical protection (passivation) of the core surface by $RS(AuSR)_x$ units, the number of which has to be "just right" so that (iii) a major gap is exposed in the electron shell structure. The resulting *superatom* is a thermodynamically stable species at ambient conditions just as the ordinary atoms in the Periodic Table.

The existence of two different protective units in $Au_{102}(p\text{-MBA})_{44}$, RSAuSR and $RS(AuSR)_2$, may seem surprising. However, polymeric "zig-zag" chains or rings of such units are known (see ref. 42 and references therein). The $RS(AuSR)_2$ unit may exist (at least) in two conformations, a sharp-angle or wide-angle "V" with the central Au–S–Au angle around 100 or 124 degrees, respectively. While the latter one was found in $Au_{102}(p\text{-MBA})_{44}$, the "sharp-angle V" unit was found to offer an ideal building block to protect a much smaller particle $Au_{25}(SR)_{18}$ where the composition could be written as $Au_{13}[RS(AuSR)_2]_6$.[48] The central Au_{13} core is a slightly distorted icosahedron with the 6 ligands octahedrally arranged around the core (Fig. 22). Taking the cluster to be anionic ($q = -1$) renders the system as an 8-electron "superatom" (the 6 $SR(AuSR)_2$ units localize in total 6 electrons from the 14-electron (6s) shell structure of Au_{13}^- and in jellium notation, the 6s-derived shells are $1S^21P^6$, see Fig. 23). It has to be noted that the $Au_{25}(SR)_{18}^q$ cluster had been known already for some years to be one of the smallest very stable all-thiolate protected gold clusters, and previous theoretical models employed the "core-in-cage" concept with a Au_7^q core.[44]

Remarkably, a simultaneous and independent experiment[49] confirmed the structural prediction for $Au_{25}(SR)_{18}^-$. The cluster was passivated by using the SCH_2CH_2Ph ligand. The unit cell of the crystal was found to contain also a TOA^+ counterion (tetraoctylammonium, a phase-transfer agent) which confirmed the anionic state of the gold cluster. The theoretical analysis revealed that the close-to-icosahedral Au_{13} is quite rigid also with respect to charge $q = 0, 1$, confirming in part the earlier experimental results that indicated the robustness of optical spectra with respect to charges $q = -1, 0, 1$.[50] The robustness can be understood straightforwardly from the superatom model (see Fig. 24): it was observed that the Au_{13} core remains rigid for different charge states, hence the major optical transitions of $q = 0, 1$ clusters are still over the

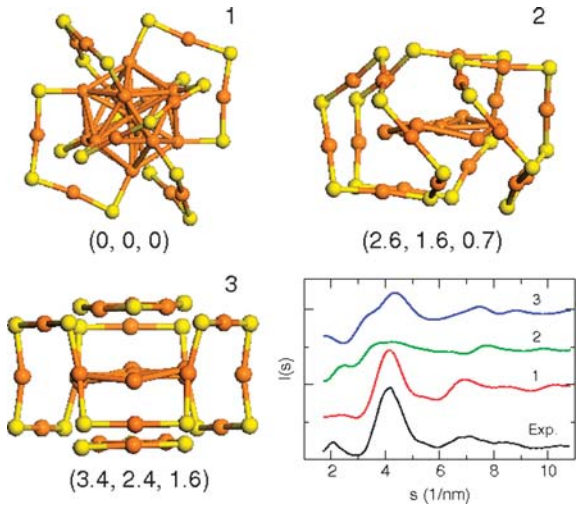

Fig. 22 Skeletal structures of three isomers for $Au_{25}(SR)_{18}^{q}$ clusters. The numbers in parentheses are energy differences to the ground state isomer 1 for charge states $q = -1$, 0, $+1$, respectively. Isomer 1 follows the "divide and protect" structure motif and is an 8-electron "superatom" in charge state $q = -1$. The bottom right panel compares XRD patterns. Reproduced from ref. 48 by permission. Copyright 2008 American Chemical Society.

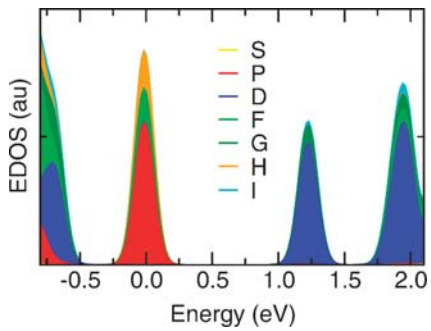

Fig. 23 Angular momentum analysis of the highest states in cluster 1 of Fig. 22. The HOMO state is at zero energy. Reproduced from ref. 48 by permission. Copyright 2008 American Chemical Society.

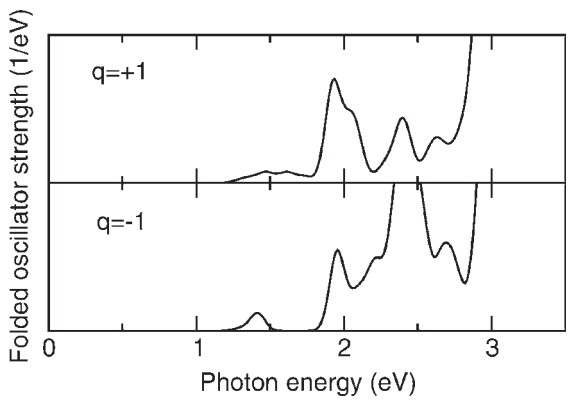

Fig. 24 Optical spectra of cluster 1 of Fig. 22 in two charge states. Reproduced from ref. 48 by permission. Copyright 2008 American Chemical Society.

"HOMO–LUMO gap" of the $q = -1$ cluster, since transitions inside the same angular-symmetric shell (1P in jellium notation) are forbidden by the dipole selection rule.[48] Soon afterwards, a more detailed analysis of the optical excitations of a model cluster $Au_{25}(SH)_{18}^{-}$ followed.[51] The observation of $Au_{25}(SR)_{18}^{-}$ added yet another member to the "family" of ligand-protected clusters with 8 delocalized electrons (see below), a family that was born by early predictions[52] and synthesis[32] of $[Au_{13}(PMe_2Ph)_{10}Cl_2](PF_6)_3$ complex.

3.4 Phosphine-stabilized Au_{11} and Au_{39} clusters: superatoms with 8 and 34 electrons

Various Au_{11} and Au_{13}-based phosphine–halide passivated clusters have been characterized in solid state by X-ray diffraction since the late 1970's (for a review, see ref. 53). The undecagold compounds generally have the formula $Au_{11}(PR_3)_7X_3$ where X = halide or thiolate, and the gold skeleton often has an approximate C_{3v} symmetry. A recent investigation[47] dealt with the electronic structure of clusters $Au_{11}(PH_3)_7(SMe)_3$ and $Au_{11}(PH_3)_7Cl_3$ which are homologous models for a recently reported thiolate-stabilized cluster $Au_{11}(S\text{-}4\text{-}NC_5H_4)_3(PPh_3)_7$.[54]

The HOMO–LUMO gaps of these compounds are 1.5 eV for X = SMe and 2.1 eV for X = Cl (Table 1). The dominant angular momentum character of the states around the gap was found to change from P-symmetry to D-symmetry. In the delocalized electron model this corresponds to closing of the 8 electron (in configuration $1S^21P^6$) gap. This gap exposure is due to the fact that the three halide or thiolate ligands localize one electron each out of the eleven conduction electrons from the gold core. It is interesting to note that a halide and a thiolate ligand act here in analogous roles, although the character of the Au–Cl bond is more "iono-covalent" than that of the Au–SR bond. The seven phosphine ligands act as weak surfactants in both systems, without modifying the electron shell structure of the gold core.

A tridecagold compound $[Au_{13}(PMe_2Ph)_{10}Cl_2][PF_6]_3$ was experimentally characterized in 1981,[32] confirming earlier theoretical predictions of stable ligand-protected icosahedral gold clusters.[52] The three hexafluorophosphate anions stabilize the triple-cationic gold compound in the crystal structure. Our calculated HOMO–LUMO gap for the homologous relaxed $Au_{13}(PH_3)_{10}Cl_2^{3+}$ compound is 1.8 eV (Table 1), very similar to the undecagold compounds.

In 1992, the $Au_{39}(PPh_3)_{14}Cl_6^{q}$ compound was isolated and crystallized, and for 15 years remained the largest "soluble" cluster with an unambiguously determined structure.[55] The geometrical arrangement of the Au_{39} core of this cluster is close to D_3 symmetry, and can be also described as two hexagonal close-packed (hcp) crystallites, joined together by a 30 degree twist (see Fig. 18). There is only one fully coordinated gold atom in the center of a hexagonal antiprismatic cage. The calculated HOMO–LUMO gap was found to be large, 0.8 eV, for the anionic compound ($q = -1$).[47] The angular momentum analysis of the electron states around the gap showed that the gap closes a band of states that have dominantly F-character while the states above the gap have a major G-character. The F-shell closing indicates an effective

Table 1 Shell closures and HOMO–LUMO gaps for ligand-protected clusters, compared to reference values deduced from photoelectron spectroscopy for gas-phase cluster anions. See section 3.5

	Experiment		Theory					
Shell closing n^*	Cluster	Gap	Cluster compound	s	N	M	q	Gap
8 ($1S^21P^6$)			$Au_{11}(PH_3)_7(SMe)_3$	7	11	3	0	1.5 eV
8			$Au_{11}(PH_3)_7Cl_3$	7	11	3	0	2.1 eV
8			$Au_{13}(PH_3)_{10}Cl_2^{3+}$	10	13	2	+3	1.8 eV
8			$Au_{25}(SMe)_{18}^-$	0	25	18	−1	1.2 eV
34 ($8 + 1D^{10}2S^21F^{14}$)	Au_{34}^-	1.0 eV	$Au_{39}Cl_6(PH_3)_{14}^-$	14	39	6	−1	0.8 eV
58 ($34 + 2P^61G^{18}$)	Au_{58}^-	0.6 eV	$Au_{102}(p\text{-MBA})_{44}$	0	102	44	0	0.5 eV
58			$Au_{102}(SMe)_{44}$	0	102	44	0	0.5 eV

conduction electron count of 34 in the gold core. This is consistent with the fact that there are six iono-covalent AuCl bonds at the surface, thereby reducing the effective count of delocalized electrons from 40 to 34.

3.5 The unifying superatom concept

The above analysis of precisely known compositions and structures of all-thiolate, phosphine–halide or phosphine–thiolate protected gold clusters suggests that all these compounds can be expressed by a formula

$$(L_s{\cdot}Au_NX_M)^q$$

where the gold cluster (size N) is protected by M electron-withdrawing ligands X (X is a halide or a thiolate) and s weak ligands L can be added to complete the chemical protection of the Au core. Ligands L are ''weak ligands'' and do not affect the effective free-electron-count of the gold core. The compound may have an overall charge q. All the shell closings (hence the electronic stability) n^* can be evaluated with an ''effective gold valence'' $v_A = 1$ from

$$n^* = Nv_A - M - q$$

The result of this analysis is summarized in Table 1. A compound having a closed electron shell and a complete chemical protection of the metal core can be called a ''noble-gas superatom''.

Traditionally, the ''phosphine chemistry'' and the ''thiolate chemistry'' have been regarded as separate branches to prepare ligand-protected gold nanoparticles; no general, unifying theoretical concepts have been available to understand and classify the wealth of experimental information on the well-defined, discrete compounds. The recent experimental and theoretical advances[45,47–49,51] now provide certain guiding principles for molecular-precision synthesis and functionalization of these exciting building blocks of nano-materials that are finding applications in diverse fields of biolabeling, photonics, sensing and nanocatalysis. The early suggestions to use ''magic'' metal clusters as ''superatoms''[56] to build novel materials may now be realized by ligand-protected gold clusters.

4. Conclusions

This review shows that while gaining the reliable, detailed information on the most-preferred atomic structures and geometries that gold clusters exhibit as bare objects or covered by ligands is a highly-nontrivial task, requiring the proper use of the (scalar)-relativistic theory, the *post-priori* analysis of the electronic structure of the most stable clusters reveals surprisingly simple rules.

The electronic stabilities can be related to pertinent Au(6s) derived free-electron-shell closings (at least) for the following bare clusters: Au_6 ($1S^21P^4$), Au_{12} ($Au_6 + 2S^21D^4$), $Au_{16}^{(2-)}$ ($1S^21P^61D^{10}$), Au_{20} ($Au_{16}^{(2-)} + 2S^2$), Au_{34} ($Au_{20} + 1F^{14}$) and Au_{58} ($Au_{34} + 2P^61G^{18}$). The shell-closings also play a major role in explaining the electronic stability of ligand-protected gold clusters, defining, *e.g.*, the character of the lowest-lying optical transitions in the gold core. It is comforting that such simple but powerful concepts hold for gold, as the theoretical understanding of guiding principles that would help in designing functional but stable gold-based components for applications in nanotechnology is in dire need. This is an issue with great theoretical challenges but bright views into future.

Acknowledgements

I wish to thank all the following scientist whose contributions to various collaborations over the past 10 years have each taught me some new aspects about the physics and chemistry of gold clusters and nanoparticles: C. Ackerson, J. Akola, R. N. Barnett, T. Bernhardt, G. Calero, C. L. Cleveland, P. Frondelius, H. Grönbeck, U. Heiz, K. Honkala, B. v. Issendorff, P. Jadzinsky, P. Koskinen, U. Landman, O. Lopez-Acevedo, K. Manninen, M. Manninen, M. Moseler, P. Pyykkö, M. Walter, L.-S. Wang, R. L. Whetten and L. Wöste. I wish to thank R. Kornberg for access to crystal-structure data of the $Au_{102}(p\text{-MBA})_{44}$ cluster before its publication in ref. 45, R. W. Murray for sending the coordinates of $[N(C_8H_{17})_4][Au_{25}(SCH_2CH_2Ph)_{18}]$ (ref. 49) and I. Garzon and K. Nobusada for sharing theoretical structures for thiolate-protected Au_{38} and Au_{25} clusters, respectively. I also wish to acknowledge the open communication with S. Gilb in 2001–2002 which facilitated comparisons of isomer structures and energy ordering of planar gold cluster anions found in the concurrent theoretical works of the Karslruhe and Atlanta groups that led to ref. 8–10. The author's work is supported by the Academy of Finland, the Finnish IT Center for Science (CSC) and the Distributed European Infrastructure for Supercomputing Applications (DEISA).

References

1 *Gold—Progress in Chemistry, Biochemistry and Technology*, ed. H. Schmidbaur, Wiley, Chichester, 1999.

2 P. Pyykkö, *Chem. Rev*., 1988, **88**, 563.
3 For reviews on gold clusters and nanoparticles, see: G. Schmid, *Chem. Rev*., 1992, **92**, 1709; M.-C. Daniel and D. Astruc, *Chem. Rev*., 2004, **104**, 293; P. Pyykkö, *Angew. Chem., Int. Ed*., 2004, **43**, 4412; P. Pyykkö, *Inorg. Chim. Acta*, 2005, **358**, 4113; P. Schwerdtfeger and M. Leinand, in *Gold Chemistry. Current trends and future directions*, ed. F. Mohr, Wiley, New York, to be published in 2009; other reviews in this issue of *Chem. Soc. Rev*.
4 For an authoritative review on the free-electron-model (''jellium'') on simple metal clusters, see: W. A. deHeer, *Rev. Mod. Phys*., 1993, **65**, 611.
5 S. Gilb, P. Weis, F. Furche, R. Ahlrichs and M. M. Kappes, *J. Chem. Phys*., 2002, **116**, 4094.
6 S. Gilb, PhD thesis, University of Karslruhe, 2001.
7 H. Häkkinen and U. Landman, *Phys. Rev. B: Condens. Matter Mater. Phys*., 2000, **62**, R2287.
8 F. Furche, R. Ahlrichs, P. Weis, C. Jacob, S. Gilb, T. Bierweiler and M. M. Kappes, *J. Chem. Phys*., 2002, **117**, 6982.
9 H. Häkkinen, B. Yoon, U. Landman, X. Li, H.-J. Zhai and L.-S. Wang, *J. Phys. Chem. A*, 2003, **107**, 6168.
10 H. Häkkinen, M. Moseler and U. Landman, *Phys. Rev. Lett*., 2002, **89**, 033401.
11 H. Grönbeck and P. Broqvist, *Phys. Rev. B: Condens. Matter Mater. Phys*., 2005, **71**, 073408.
12 M. Walter and H. Häkkinen, *New J. Phys*., 2008, **10**, 043018.
13 K. J. Taylor, C. L. Pettiette-Hall, O. Cheshnovsky and R. E. Smalley, *J. Chem. Phys*., 1992, **96**, 3319.
14 O. Kostko, PhD thesis, University of Freiburg, 2007.
15 P. Koskinen, H. Häkkinen, B. Huber, B. v. Issendorff and M. Moseler, *Phys. Rev. Lett*., 2007, **98**, 015701.
16 M. P. Johansson, A. Lechtken, D. Schooss, M. M. Kappes and F. Furche, *Phys. Rev. A: At., Mol., Opt. Phys*., 2008, **77**, 053202.
17 B. Yoon, P. Koskinen, B. Huber, O. Kostko, B. v. Issendorff, H. Häkkinen, M. Moseler and U. Landman, *ChemPhysChem*, 2007, **8**, 157.
18 E. Janssens, H. Tanaka, S. Neukermans, R. E. Silverans and P. Lievens, *New J. Phys*., 2003, **5**, 46.
19 M. Walter, P. Frondelius, K. Honkala and H. Häkkinen, *Phys. Rev. Lett*., 2007, **99**, 096102.
20 X. Xing, B. Yoon, U. Landman and J. H. Parks, *Phys. Rev. B: Condens. Matter Mater. Phys*., 2006, **74**, 165423.
21 S. Bulusu, X. Li, L.-S. Wang and X. C. Zeng, *Proc. Natl. Acad. Sci. U. S. A*., 2006, **103**, 8326.
22 J. Li, X. Li, H.-J. Zhai and L.-S. Wang, *Science*, 2003, **299**, 864.
23 I. Opahle, PhD thesis, Technical University of Dresden, 2001.
24 M. Walter and H. Häkkinen, *Phys. Chem. Chem. Phys*., 2006, **8**, 5407.
25 M. P. Johansson, D. Sundholm and J. Vaara, *Angew. Chem., Int. Ed*., 2004, **43**, 2678.
26 J. Wang, J. Jellinek, J. Zhao, Z. Chen, R. B. King and P. von Ragué Schleyer, *J. Phys. Chem. A*, 2005, **109**, 9265.
27 A. J. Karttunen, M. Linnolahti, T. A. Pakkanen and P. Pyykkö, *Chem. Commun*., 2008, 465.
28 A. Lechtken, D. Schooss, J. R. Stairs, M. N. Blom, F. Furche, N. Morgner, O. Kostko, B. von Issendorff and M. M. Kappes, *Angew. Chem., Int. Ed*., 2007, **46**, 2944.
29 Y. Kondo and K. Takayanagi, *Science*, 2000, **289**, 606.
30 H. Häkkinen, M. Moseler, O. Kostko, N. Morgner, M. A. Hoffmann and B. v. Issendorff, *Phys. Rev. Lett*., 2004, **93**, 093401.
31 G. Schmid, R. Pfeil, R. Boese, F. Bandermann, S. Meyer, G. H. M. Calis and J. W. A. van der Velden, *Chem. Ber*., 1981, **114** 3634.
32 C. E. Briant, B. R. C. Theobald, J. W. White, L. K. Bell and D. M. P. Mingos, *J. Chem. Soc., Chem. Commun*., 1982, 201.
33 M. Brust, M. Walker, D. Bethell, D. J. Schiffrin and R. J. Whyman, *J. Chem. Soc., Chem. Commun*., 1994, 801.
34 R. L. Whetten, J. T. Khoury, M. M. Alvarez, S. Murthy, I. Vezmar, Z. L. Wang, P. W. Stephens, C. L. Cleveland, W. D. Luedtke and U. Landman, *Adv. Mater*., 1996, **8**, 428.
35 C. L. Cleveland, U. Landman, T. G. Schaaff, M. N. Shafigullin, P. W. Stephens and R. L. Whetten, *Phys. Rev. Lett*., 1997, **79**, 1873.
36 H. Häkkinen, R. N. Barnett and U. Landman, *Phys. Rev. Lett*., 1999, **82**, 3264.
37 R. N. Barnett, C. L. Cleveland, H. Häkkinen, W. D. Luedtke, C. Yannouleas and U. Landman, *Eur. Phys. J. D*, 1999, **9**, 95.
38 H. Grönbeck and W. Andreoni, *Int. J. Quantum Chem*., 2000, **80**, 598.
39 I. L. Garzón, C. Rovira, K. Michaelian, M. R. Beltrán, P. Ordejón, J. Junquera, D. Sánchez-Portal, E. Artacho and J. M. Soler, *Phys. Rev. Lett*., 2000, **85**, 5250.
40 I. L. Garzón, K. Michaelian, M. R. Beltrán, A. Posada-Amarillas, P. Ordejón, E. Artacho, D. Sánchez-Portal and J. M. Soler, *Phys. Rev. Lett*., 1998, **81**, 1600.
41 H. Häkkinen, M. Walter and H. Grönbeck, *J. Phys. Chem. B*, 2006, **110**, 9927.
42 H. Grönbeck, M. Walter and H. Häkkinen, *J. Am. Chem. Soc*., 2006, **128**, 10269.
43 D. Kruger, H. Fuchs, R. Rousseau, D. Marx and M. Parrinello, *Phys. Rev. Lett*., 2002, **89**, 186402.
44 T. Iwasa and K. Nobusada, *J. Phys. Chem. C*, 2007, **111**, 45.
45 P. D. Jadzinsky, G. Calero, C. J. Ackerson, D. A. Bushnell and R. D. Kornberg, *Science*, 2007, **318**, 430.
46 R. Price and R. L. Whetten, *Science*, 2007, **318**, 407.
47 M. Walter, J. Akola, O. Lopez-Acevedo, P. D. Jadzinsky, G. Calero, C. J. Ackerson, R. L. Whetten, H. Grönbeck and H. Häkkinen, *Proc. Natl. Acad. Sci. U. S. A*., 2008, **105**, 9157.
48 J. Akola, M. Walter, R. L. Whetten, H. Häkkinen and H. Grönbeck, *J. Am. Chem. Soc*., 2008, **130**, 3756.
49 M. W. Heaven, A. Dass, P. S. White, K. M. Holt and R. W. Murray, *J. Am. Chem. Soc*., 2008, **130**, 3754.
50 Y. Negishi, N. K. Chaki, Y. Shichibu, R. L. Whetten and T. Tsukuda, *J. Am. Chem. Soc*., 2007, **129**, 11322.
51 M. Zhu, C. M. Aikens, F. J. Hollander, G. C. Schatz and R. Jin, *J. Am. Chem. Soc*., 2008, **130**, 5883.
52 D. M. P. Mingos, *J. Chem. Soc., Dalton Trans*., 1976, 1163.
53 D. M. P. Mingos in ref. 1.
54 K. Nunokawa, S. Onaka, M. Ito, M. Horibe, T. Yonezawa, H. Nishihara, T. Ozeki, H. Chiba, S. Watase and M. Nakamoto, *J. Organomet. Chem*., 2006, **691**, 638.
55 B. K. Teo, X. Shi and H. Zhang, *J. Am. Chem. Soc*., 1992, **114**, 2743.
56 S. N. Khanna and P. Jena, *Phys. Rev. Lett*., 1992, **69**, 1664.